Journal of Molecular Structure 1199 (2020) 126938

Contents lists available at ScienceDirect

Journal of Molecular Structure

journal homepage: http://www.elsevier.com/locate/molstruc

Synthesis, structural characterization and anti-breast cancer activity evaluation of three new Schiff base metal (II) complexes and their nanoparticles

Di Wu [a], Liang Guo [b], Si-Jie Li [a, *]

[a] Department of Breast Surgery, The First Hospital of Jilin University, Changchun, Jilin, China
[b] Department of Pathology, The First Hospital of Jilin University, Changchun, Jilin, China

ARTICLE INFO

Article history:
Received 18 June 2019
Received in revised form
15 August 2019
Accepted 17 August 2019
Available online 19 August 2019

Keywords:
Coordination complexes
Cu(II) chelating
Ni(II) chelating
Nanoparticles
Breast cancer
Proliferation
Apoptosis
ROS

ABSTRACT

Two Schiff base ligands 2-((ethylamino)methyl)-6-methoxyphenol (HL_1) and (E)-2-(((2-(dimethylamino) ethyl)imino)methyl)-6-methoxyphenol (HL_2) with bi-nucleating or tri-nucleating mode have been successfully prepared via an one step organic condensation reaction, which were further applied in the synthesis of three new Cu(II) and Ni(II)-based coordination complexes $[Cu(L_1)_2](EtOH)$ (**1**), $[Ni(L_1)_2](EtOH)$ (**2**) and $[Cu(L_2)(HL_2)(SCN)](MeOH)_2$ (**3**). Furthermore, a hand grinding technique has been used to decrease the particle diameter of complexes **1**–**3**, thus forming nano-complexes. In biological activity research, we revealed the important function of nanoparticle **1** in the treatment of breast cancer. Mitochondria is critical in generating intracellular energy, and play a vital role in regulating cells life and death. Therefore, the apoptosis of MCF7 breast cancer cells after treated with nanoparticles was detected by Annexin V-FITC/PI method. The results showed that nanoparticles **1** could significantly raise apoptotic cells number, but not nanoparticles **2**–**3**. Moreover, we assessed the mitochondrial membrane potential and reactive oxygen species (ROS) in MCF7 cancer cells, finally we draw this conclusion, nanoparticle **1** could damage the mitochondrial membrane, leading increased ROS level, and cause the apoptotic cell death.

1. Introduction

Metal compounds have attracted wide attention due to their applications in bactericidal, anticancer and flame retardant fields [1–5]. The success of coordination metal complexes in cancer chemotherapy has been demonstrated by Cisplatin, which is still one of the most effective and world's best-selling anticancer drug [6–9]. However, the Cisplatin and its analogic drugs (such as Carboplatin and Oxaliplatin) are limited by the serious side effects, general toxicity, and drug resistance, which restrict their high-dose administration [10]. In recent years, drug and bioinorganic chemists have designed novel metal-based anticancer agents due to obvious clinical problems of chemotherapeutic drugs. These anticancer agents have the characteristics of low toxicity, good selectivity and biological activity [11]. Myocardial dysfunction is getting more and more attention of researchers, which is related with many diseases. During the pathogenesis of myocardial dysfunction, the increased level of ROS accumulation in cells will lead to the cell apoptosis via the caspase mediated singling pathway.

Schiff base compounds are usually regarded as "privileged ligands" due to they are easily prepared by the condensation reaction between imines and aldehydes. Schiff base ligands can not only coordinate with various metal ions, but also stabilize them in different oxidation states. Schiff bases have the characteristics of imino NCH, it is helpful to elucidate the mechanism of Schiff racemization and transamination. In recent 20 years, the chemical research of nitrogen-containing Schiff base metal complexes and their donors has attracted wide attention because of their broad application prospects, such as antituberculosis, antineoplastic, antimalarial, anticancer, antioxidant, antifungal, and anticonvulsant, corrosion inhibition as well as anti-inflammatory activity [12–16]. Bidentate Schiff and the tridentate Schiff ligands have been widely used in the construction of coordination complexes which has various clinical and biological applications [17,18]. On the other hand, Cu(II)-based coordination complexes have cytotoxic, antiproliferative, genotoxic and antitumour activities. Another

* Corresponding author.
E-mail address: sijie_li666@126.com (S.-J. Li).

https://doi.org/10.1016/j.molstruc.2019.126938
0022-2860/

driving force for the employment of Cu (II) ion is its low toxicity, which can be further reduced by formation of the coordination complexes. In addition, Cu (II) complexes have been used as anticancer agents because of their permeability selective to cancer cell membranes, and many of these complexes are active against platinum-resistant cancer cell lines [19,20]. Besides, recent literatures have shown that some Ni(ll)-based complexes also reveal potential anticancer activities [21–23]. In the design of metal-organic anticancer drugs, the effects of the metal ions and the organic ligands are two key factors which contribute to the anticancer activity of the targeted anticancer drugs. To study the coordination surrounding along with the metal type effects on the anticancer activity of the resulting metal-organic complexes, in this research, two Schiff base ligands 2-((ethylamino)methyl)-6-methoxyphenol (HL_1) and (E)-2-(((2-(dimethylamino)ethyl) imino)methyl)-6-methoxyphenol (HL_2) with bi-nucleating or tri-nucleating mode have been successfully prepared via an one step organic condensation reaction, which were further applied in the synthesis of three new Ni(II) and Cu(II)-containing coordination complexes $[Cu(L_1)_2](EtOH)$ (**1**), $[Ni(L_1)_2](EtOH)$ (**2**) and $[Cu(L_2)(HL_2)(SCN)](MeOH)_2$ (**3**) (Scheme 1). Furthermore, the green grinding technique has been used to decrease the particle diameter of complexes **1**–**3**, thus forming nano-complexes. We also evaluated the cell viability and proliferation of MCF7 human breast cancer cells after treated with nanoparticles **1**–**3**. Firstly, we evaluated the anticancer effect of nanoparticles **1**–**3** on MCF7 cells with CCK-8 assay, results indicated only nanoparticle **1** could inhibit the proliferation and activity of MCF7 cells, and had no cytotoxicity to normal human cells. Further, we convinced that nanoparticle **1** could induce apoptosis and ROS accumulation in MCF7 cells by triggering mitochondrial fragmentation. In general, these findings mainly reflect that the compound has good anticancer activity in the treatment of human breast cancer.

2. Experimental

2.1. Chemicals and measurements

All chemicals were available on the market and were utilized with no further purified. DMSO was applied as the solvent medium in the biological studies. We prepared the two organic ligands by utilizing the literature approach [24]. The elements of N, H and C were analyzed by Perkinelemer 240C analyzer. PE diamond thermogravimetric analyzer was used for thermogravimetric analysis in nitrogen atmosphere with heating rate of 10 C/min. On a Rigaku Dmax 2500 diffractometer which has Cu-Kα radiation (λ = 1.5418 Å), we carried out the powder X-ray diffraction analyses. We determined the morphology of the nanostructured compound (S-4200, Hitachi, Japan) via scanning electron microscopy. Ultrasound was produced via a multi-wave KQ2200DE with 40 kHz frequency. Fourier transform infrared data were obtained from KBr pellets in the range of 4000–400 cm^{-1} on a 2000 spectrometer (Fig. S1). On a PerkinElmer lambda which is 35 ultraviolet–visible spectrophotometer we recorded the electronic spectra (Fig. S2).

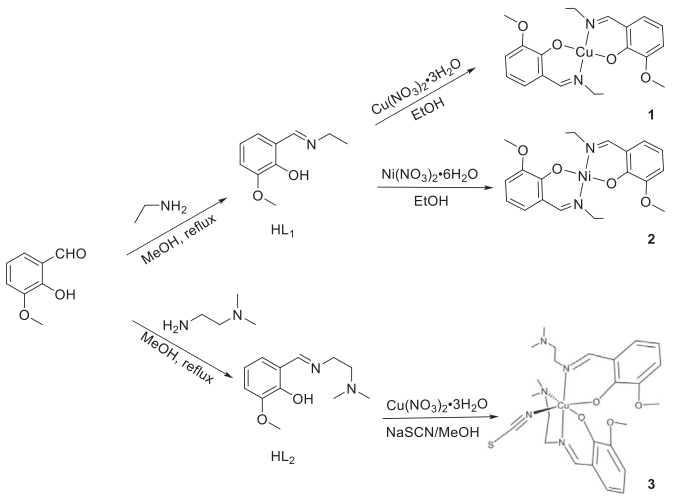

Scheme 1. The synthesis routes for the complexes **1**–**3**.

The normal lung cell line BEAS-2B and human breast cancer cell line MCF7 was purchased from American Type Culture Collection (ATCC, Rockville, MD), then cultured in ATCC-formulated RPMI-1640 (Gibco, NY, USA) and Dulbecco's modified Eagle's medium (DMEM; Gibco, NY, USA), respectively. 2% L-glutamine, 10% (V/V) heat inactivated fetal bovine serum (FBS) as well as 100 U/mL penicillin Streptomycin Solution were added to the culture medium. The cells were cultured at 5% CO_2, 37 °C. On the basis of the cell states, the culture medium was replaced, followed by passage when 80% of them were fused.

2.2. Preparation of complexes 1–3

For complex **1**, we added $Cu(NO_3)_2 \cdot 3H_2O$ which is 0.24 g and 1 mmol and Schiff base ligand HL_1 which is 0.181 g and 1 mmol into ethanol solution of 20 mL and mixed them fully by magnetic stirring. The mixture was cooled to room temperature after reflux for 2 h. We filtered the blue precipitation of Cu(II) complex which we obtained, then washed it in cold ethanol of 15 mL, and dried by anhydrous $CaCl_2$ in vacuum. The obtained solid was then dissolved in the acetonitrile and then kept silence for two weeks to afford the single crystals of complex **1** suitable for X-ray diffraction. Yield: 160 mg (41%, based on $Cu(NO_3)_2 \cdot 3H_2O$). Anal. Calc for **1** ($C_{22}H_{30}CuN_2O_5$): C, 56.70; H, 6.49; N, 6.01%. Found: C, 56.59; H, 6.36; N, 5.94%. UV–Vis: λ_{max} (nm) (ε, M^{-1}, cm^{-1}) (CH_3OH): 233 (6.7×10^3), 268 (3.6×10^3), 333 (2.4×10^3), 410 (1.4×10^3).

The synthesis method of complex **2** was similar to that of complex **1** except $Ni(NO_3)_2 \cdot 6H_2O$ which is 0.29 g and 1 mmol has been used to replace the $Cu(NO_3)_2 \cdot 3H_2O$. Yield: 201 mg (53%, based on $Ni(NO_3)_2 \cdot 3H_2O$). Anal. Calc for **2** ($C_{22}H_{30}N_2NiO_5$): C, 57.30; H, 6.56; N, 6.07%. Found: C, 56.68; H, 6.62; N, 6.01%. UV–Vis: λ_{max} (nm) (ε, M^{-1}, cm^{-1}) (CH_3OH): 231 (1.2×10^4), 270 (6.6×10^3), 340 (2.8×10^3), 430 (1.4×10^3), 540 (9.5×10^2).

For complex **3**, we added NaSCN which is 0.08 g and 1 mmol as well as HL_2 which is 0.448 g and 2.0 mmol to CH_3OH of 20 ml and dissolved them. Then we put the required metal salt $Cu(NO_3)_2 \cdot 3H_2O$ which is 0.24 g and 1 mmol) to CH_3OH of 20 mL. The solution was refluxed for about 3 h. After the methanol solution was cooled to room temperature, the blue bulk single crystal of **3** was acquired by slow evaporation. Yield: 201 mg (53%, based on $Cu(NO_3)_2 \cdot 3H_2O$). Anal. Calc for $C_{27}H_{42}CuN_5O_6S$: C, 51.62; H, 6.74; N, 11.15%. Found: C, 51.26; H, 6.26; N, 11.23%. UV–Vis: λ_{max} (nm) (ε, M^{-1}, cm^{-1}) (CH_3OH): 230 (1.3×10^4), 270 (6.8×10^3), 342 (2.4×10^3), 426 (1.5×10^3), 570 (1.9×10^3).

The prepared complexes **1**–**3** were dissolved in 1% DMSO for further experiment.

2.3. Crystal structure and refinement

Using a Xcalibur, Eos Gemini CCD diffractometer (Agilent Technologies Inc) equipping graphite-monochromatized Enhance (Mo) X-ray Source (λ = 0.71073 Å) and φ–ω scan technology to collect the single-crystal data for compounds **1**–**3**. The data was

compressed by the bruker-saint package to generate hkl file. SADABS program is used for absorption correction. The structure of anisotropic non-hydrogen atoms was further refined by utilizing the SHELXL software (version_number: 2018/3) on F^2 after solving the direct method on the basis of the SHELXS software [25]. By utilizing the riding model, H atoms were added to the calculations. For the highly disordered nature of the lattice solvents, they could not be figured out from the electron density map via the structural refinement, and their detailed information has been determined via the elemental analysis and TGA data [26,27]. The refinement results and crystallographic parameters are summarized in Table 1.

2.4. Anti-proliferation assay by CCK-8

To examine whether nanoparticles **1**–**3** could cause the death of MCF7 cancer cells, we used serious doses of nanos to treat cells for 24 h. The cell Counting Kit-8 (CCK-8) used in this experiment was acquired from Japan Dojindo. According to the scheme, we tested the survival rate and proliferation rate of normal lung cell line BEAS-2B and human breast cancer cell line MCF7 after 24 h treatment by nanoparticles **1**–**3** [28]. Briefly, MCF7 and BEAS-2B cells at logarithmic growth stage were planted on 96-well plate at 1×104 cells per well, and cultured in 37 °C and 5% humidified CO_2 condition. When the cells achieved 70%–80% confluence, the cells were treated with **1**–**3** (1, 2, 4, 8, 10, 20, 40, 80, 100 μM) consistence of nanoparticles for 24 h. Then, we removed the culture medium, and the cells were washed three times with pre-sealed PBS. CCK8 (Sigma) was cultured in 100 μL medium without FBS. The cells were cultured in darkness for 2 h. The cells number in the three holes was measured by absorption spectrophotometry of monosodium salts with WST-8 (2-(2-methoxy-4-nitrobenzene)-3-(4-nitrobenzene)-5-(2,4-disulfonophenyl) -2H tetrazole reduced at 450 nm. The cell proliferation rate was calculated according to the measured optical density (OD) value. All experiments needed to be repeated three times. Used SPSS version 22.0 to calculate IC_{50} value.

2.5. Cell apoptosis detection

On the basis of producer' instructions, apoptotic MCF7 cancer cells percentage was determined with the Annexin V-FITC/PI apoptosis detection Kit (BioVision, Mountain View, CA, USA) [29]. In brief, we collected MCF7 cancer cells and inoculated them on a 6-well culture plate at the concentration of 2×10^5 cells per well. The culture method is described above. The cells were separated into different groups, then treated them utilizing nanoparticles **1**–**3** ($1 \times IC_{50}$) for 24 h, respectively. Apoptosis inducer kit and dimethyl sulfoxide were utilized as the positive and negative contrast. After treatment, the cells were gained with 0.25% w/v trypsin and washed three times with phosphate buffer at 4 °C. Then, Annexin V-FITC and PI were stained in 100 μL 1 × Binding Buffer and cultured in dark at room temperature for 15 min. After washing with PBS twice, the stained cells were determined by flow cytometry (BD, NJ, USA) at 488 nm excitation wavelength and 525 and 625 nm emission wavelength utilizing the flow cytometry. Apoptotic analysis was performed in three independent experiments.

2.6. Cell cycle assay

Apoptotic cells often combined with cell cycle arrest. So, we detect the influence of nano **1**–**3** on the cancer cell cycle of MCF7. Propidium iodide (PI) (BD Bioscience, USA) was used for cell cycle analysis in this experiment following the instructions [30]. In brief, the MCF7 cancer cells were fostered and treated with an indicated concentration of nanoparticles **1**–**3** as described above. After that, the cells were digested, washed with the cold PBS, and fixed overnight with 75% ethanol at −20 °C. 500 μL PI solution was added for incubation for 15 min and collected for flow cytometric analysis. All experiments needed to be performed at least three times.

2.7. Mitochondrial membrane potential assay

As mentioned above, we utilize JC-1 dye to analyze the changes in mitochondrial membrane potential [31]. MCF7 cancer cells were cultured overnight at 5% humidified CO_2 in a 6-well culture plate with a concentration of 1×10^6 cells/pore at 37° Celsius. The cells were then treated with 1–3 nanoparticles at a specified concentration for 24 h. After treatment, cells were dyed with 1 μg/ml JC-1 dye at 37 °C for 20 min to avoid illumination. Then trypsinized, harvested, and used PBS to wash the cells, and subjected to flow cytometry analysis.

Table 1
Refinement and Structural parameters indexes for complex **1**–**3**.

Identification code	1	2	3
Empirical formula	$C_{20}H_{24}CuN_2O_4$	$C_{20}H_{24}N_2NiO_4$	$C_{25}H_{34}CuN_5O_4S$
Formula weight	419.95	415.12	564.17
Temperature/K	150.15	150.15	293(2)
Crystal system	monoclinic	orthorhombic	triclinic
Space group	$P2_1/c$	$P2_12_12$	$P\text{-}1$
a/Å	10.9632(7)	9.8663(3)	9.6870(9)
b/Å	10.4428(3)	23.424(2)	10.3590(10)
c/Å	9.6135(3)	4.912(3)	17.3597(15)
α/°	90	90	101.621(8)
β/°	96.892(5)	90	96.025(8)
γ/°	90	90	107.117(8)
Volume/Å^3	1092.66(8)	1135.2(7)	1605.4(3)
Z	2	2	2
ρ_{calc}g/cm^3	1.276	1.214	1.167
μ/mm^{-1}	1.024	0.878	0.778
Data/restraints/parameters	2714/1/126	2526/0/125	8913/2/331
Goodness-of-fit on F^2	1.096	1.000	1.026
Final R indexes [$I \geq 2\sigma$ (I)]	$R_1 = 0.0517$, $\omega R_2 = 0.1590$	$R_1 = 0.0597$, $\omega R_2 = 0.1341$	$R_1 = 0.1072$, $\omega R_2 = 0.2786$
Largest diff. peak/hole e Å^{-3}	1.08/-1.01	1.12/-0.87	1.67/-1.07
CCDC	1906552	1906553	1906554

2.8. Intracellular ROS detection

The accumulation of ROS in cells was measured by fluorescent probe 2,7-Dichlorofluorescein diacetate. In the present of ROS. The 2′,7′-dichloro fluorescin diacetate could be translated into 2′,7′-dichloro fluorescin, and usually as the index of intracellular ROS production [29]. In this study, 5 μmol/L DCFH-DA was pre-loaded in 37 °C alkaline medium for 30 min, using serum-free medium to wash 3 times, and treated with various nanoparticles **1**–**3**. Flow cytometry was used to detect the fluorescence of ROS in each group at 488/530 nm excitation wavelength, and the fluorescence was analyzed by FlowJo 7.6 software. All experiments need to be done three or more times.

2.9. Statistical analysis

In this study, all required experiments were conducted in triplicate form, and the data were exhibited in the form of mean ± standard deviation (SD) in three independent experiments. Utilizing student's t-test to compare the two groups, and using one-way ANOVA to compare Prism Software with more than three groups. When $^{***}p < 0.005$, $^{**}p < 0.01$ as well as $^{*}\ p < 0.05$, we considered the differences were remarkable.

3. Results and discussion

3.1. Molecular structure and characterization for complexes 1-3

Refluxing ethylamine and 2-hydroxy-3-methoxybenzaldehyde in the ethanol solution for 3 h to afford the HL_1 ligand, which is white solid after the removal of the solvents via the rotary evaporation. In CH_3CN solution, single crystals of complex **1**–**2** were acquired by slowly evaporating the mixture of HL_1 and $Cu(NO_3)_2 \cdot 3H_2O$. The prepared metal-organic complexes are soluble in dimethyl sulfoxide, ethanol, methanol, acetone, acetonitrile and other common solvents. Elemental analysis of metal complexes **1**–**2** showed that the ratio of M(II) ion to Schiff base ligand HL_1 is 1:2. The phase purity of the two as-prepared crystalline products is confirmed via the PXRD measurements and their atomic arrangements are established via the structural solution and refinements and structural solution on the basis of the corresponding crystal data. The single crystal X-ray diffraction study reveal that complex 1 belongs to the monoclinic crystal system with the space group $P2_1/c$ and demonstrates a mononuclear structure. The data collection and refinement parameters are listed in Table 1. As shown in Fig. 1a, the basic molecular repeating unit of **1** is composed of one L_1^- ligand and a half of crystallographically independent Cu (II) ion. The coordinate geometry of the central Cu (II) ion is completed by two N atoms (N1 and N1A) as well as two O atoms (O1 and O1A) from two different L_1^- ligands, which forms a completely square plane coordinate geometry (Fig. 1b). The distances of all the Cu(II)–O as well as Cu(II)–N bond are in the normal ranges, and are comparable with those of similar compounds in the literature [13,14]. As for the L_1^- ligand, its azomethine (N1–C8) bond length is 1.265(3) Å, which is in the range characteristic of C=N values. C9–H9A···O1 forms an intramolecular hydrogen bond interaction which could further stabilize the whole network. The packing of the structure of **1** results in a 3D supremolecular structure with a solvent accessible free void of 19.1% as showed by the software PLATON, which is stabilized by CH···π and CH···O weak interactions (Fig. 1c).

Complex **2** is a mononuclear complex and its structure is characterized by single crystal X-ray crystallography, which reveals that it shows a similar atomic arrangement with complex **1** but with different coordination surrounding for the centered metal ion. The

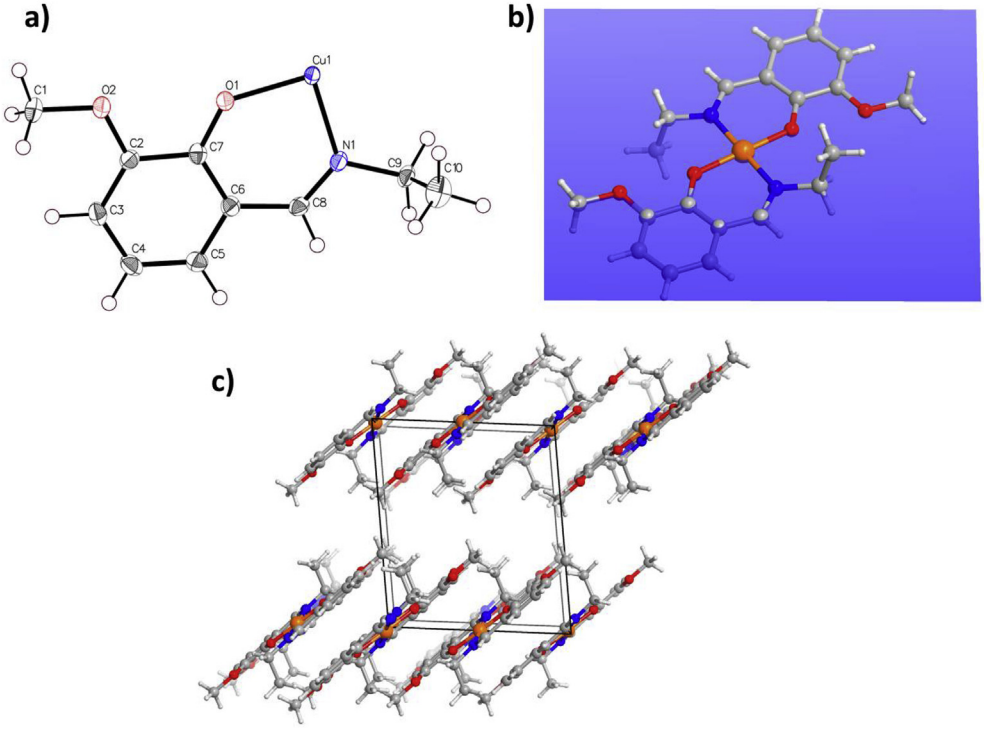

Fig. 1. (a) 1's asymmetric unit view (generated using the OLEX 2). (b) View around the plane coordinates of Cu(II) ions in **1** (generated using the Diamond 3.2k). (c) **1**'s 3D packing diagram view (generated using the Diamond 3.2k).

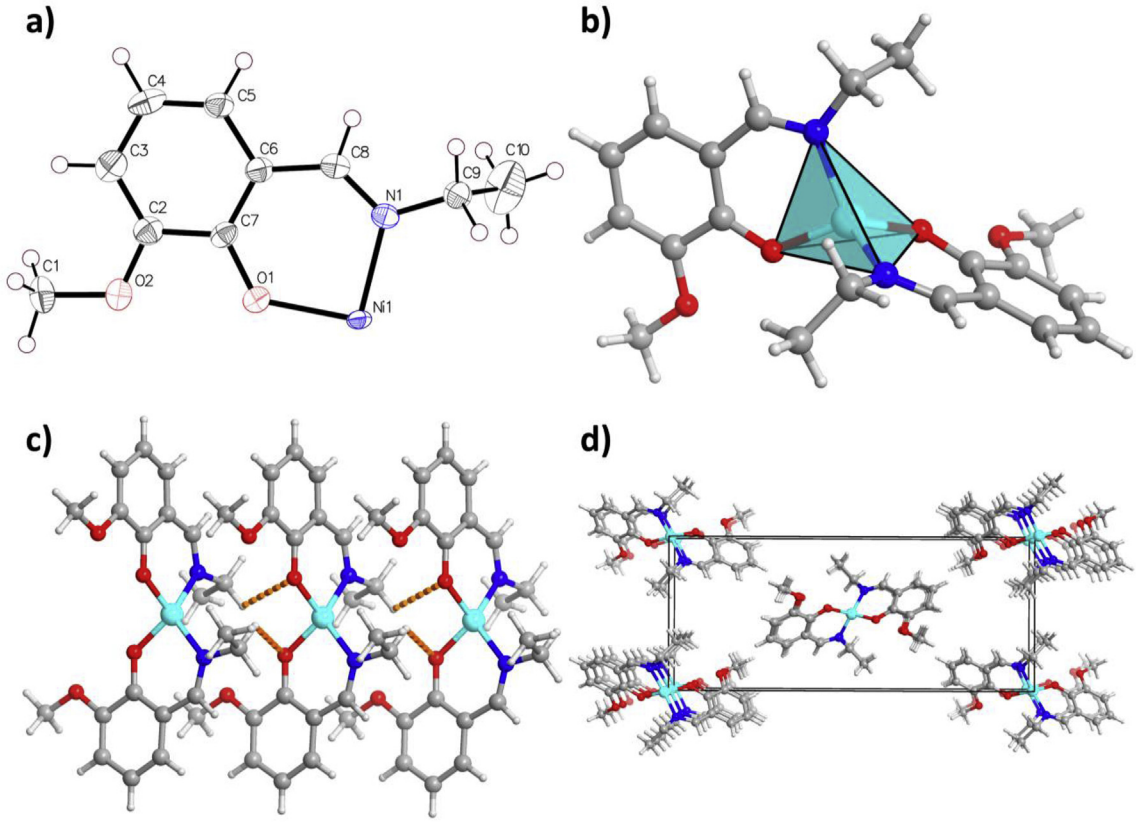

Fig. 2. (a) 2′ s asymmetric unit view (generated using the OLEX 2). (b) View of coordination mode for Ni(II) ion in **2** (generated using the Diamond 3.2k). (c) View of H-bond interaction in **2** (generated using the Diamond 3.2k). (d)**2**′ s 3D packing diagram view (generated using the Diamond 3.2k).

structural solution and the refinement results demonstrate that complex **2** locate in the orthogonal space group $P2_12_12$ and behave as a discrete structure. The asymmetric unit of **2** consists of a Schiff base ligand and a Ni (II) ion (Fig. 2a). The coordination environment of Ni(II) ion is finished by two phenoxido-O-donors of O1 and O1A as well as two imine N-donors of N1 and N1A from two Schiff base ligands, resulting in a tetrahedral geometry (Fig. 2b). All the distances of Ni(II)—N as well as Ni(II)—O bond are in normal ranges and are comparable with those of similar compounds on the basis of N,O-donor Schiff base ligands in the literatures [8—10]. Two phenoxy oxygen atoms satisfy the double positive charge of Ni (II) ion. Compound **2** has a C_2 axis in which Ni (II) ions are located in the symmetric center. The planes angle N1—Ni—O1 with N1A—Ni1—O1A is 89.12°, which means the flat tetrahedral geometry. As for L_1^- ligand, its azomethine (N1—C8) bond length is 1.271(3) Å, which is in the range characteristic of C═N values. Complex **2** forms 1D H-bonding network along c axis, involving the C9—H9A···O1 interactions with the distance of donor-acceptor is 2.152 Å (Fig. 2c). The packing of the structure of **2** results in a 3D supremolecular structure with a solvent accessible free void of 25.1% as showed by software PLATON, which is stabilized by CH···π and CH···O weak interactions (Fig. 2d).

A yellow solid ligand (E)-2-(((2-(dimethylamino)ethyl)imino) methyl)-6-methoxyphenol (HL_2) was obtained by refluxing N, N-dimethyl-1, 2-diaminoethane and 3-methoxysalicylaldehyde in the methanol solution for 1 h. The acquired ligand were directly utilized for preparing targeted Cu(II) coordination complexes. Furthermore, the +2 oxidation state of the Cu(II) ion has been confirmed via the bond valence sum (BVS) calculation, which affords a total value of 2.04 for the Cu(II) ion [32]. According to the literature, the six-coordinated octahedral coordination environment is usually found for the Cu ion with +2 oxidation state, while the Cu ion with +1 oxidation state usually has the coordination numbers less than five [33—35]. The analysis results of single crystal X-ray show that the ligand to metal stoichiometry for complex **3** is 2:1. The X-ray single crystal diffraction study reveals that complex **3** belongs to the triclinic system of space group P-1. The perspective and selective atomic numbering scheme of the complexes are shown in Fig. 3a. It shows that there is one L_2^- ligand, one HL_2 ligand, one Cu (II) ion as well as one coordinated SCN^- group in the molecular unit. The structure of the complex composes of a distorted octahedral geometry of hexacoordinated Cu(II) ion, whose coordination environment is formed by two phenoxy oxygen, two imine nitrogen atoms and a amine nitrogen atom from two demodified Schiff base ligands. Thiocyanate nitrogen atoms occupy the sixth coordination position of Cu (II), thus completing the distorted octahedral geometry of Cu (II). The octahedron equatorial plane is composed of phenoxy atom, imine-nitrogen atom as well as amine-nitrogen atom, while the thiocyanate-nitrogen atom and phenoxy-oxygen atom are the axial coordinates. An interesting finding is that the bond length of the equatorial part is longer than its axial bond length. This may be due to the steric hindrance around the metal center. Bidentate binding model of tridentate Schiff base is the most interesting structural characteristic of the complex. This keeps the Schiff base still pendant. There is a difference between the ideal value and the bond angle (90, 180), which clearly shows the deformation of octahedral geometry. The bond length of the Cu(II)—N amine is longer than that of the Cu(II)—N imine, which was also found in previously reported analogous complexes on the basis of N, O - donor Schiff base ligands [13—16]. The bond length Cu(II)—N imine in tridentate bonded Schiff bases is slightly shorter than that in bidentate

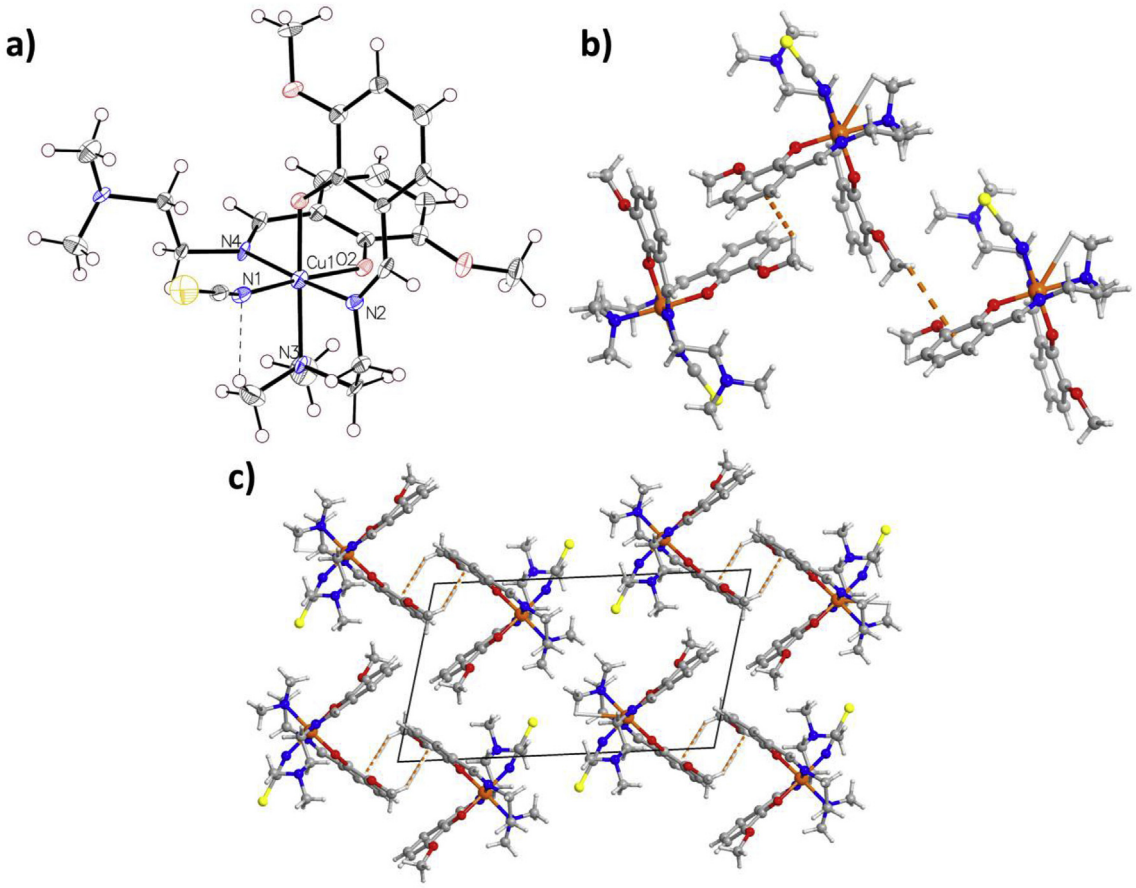

Fig. 3. (a) **3**'s asymmetric view (generated using the OLEX 2). (b) View for the C—H···π interactions in **3** (generated using the Diamond 3.2k). (c) **3**'s 3D packing diagram view (generated using the Diamond 3.2k).

bonded Schiff bases. The complex exhibits obvious C—H···π interactions (Fig. 3b). The H atom on the methoxyl group participates in inter-molecular C—H···πinteraction with the benzene ring (C1—C2—C3—C4—C5—C6). Owing to the forms of inter-molecular C—H···πinteraction, in the complex crystal packing, a one-dimensional array is formed (Fig. 3c).

3.2. PXRD, TGA and SEM characterizations

In order to examine the phase purity of the Schiff base complexes **1**–**3** prepared, their PXRD patterns were collected using their freshly prepared crystalline samples at room temperature. According to the information in Fig. 4a, the resulting PXRD curves are all consistent with those calculated from their corresponding crystal data, confirming the bulk phase purity of as-prepared three complexes. Thermogravimetric analysis (TGA) was carried out to probe their thermodynamic stability along with the information of the lattice guests (Fig. 4b). For complex **1**, 9.46% weight loss could be found between the temperature of 25 and 140 °C, which could be regarded as the result of the removal of one lattice EtOH

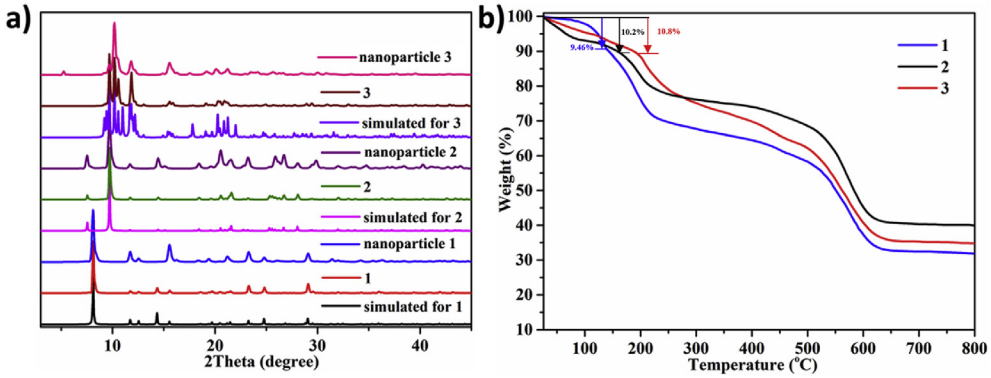

Fig. 4. (a) Complexes **1**–**3**'s PXRD patterns; (b) Complexes **1**–**3**'s TGA curves.

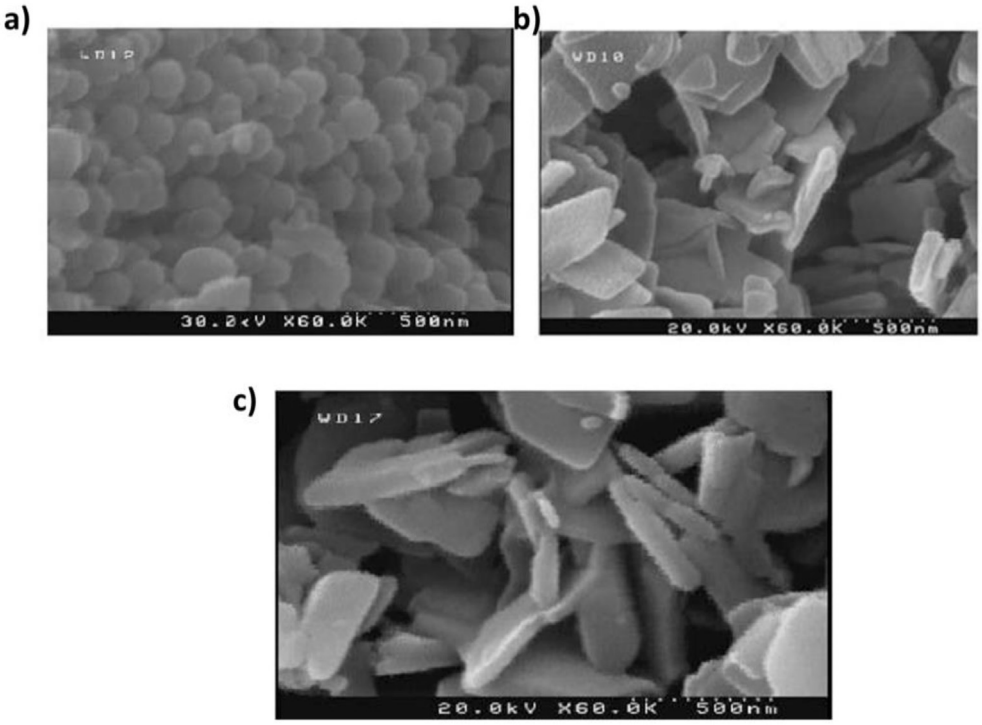

Fig. 5. The SEM images of nanoparticles **1** (a), **2** (b) and **3** (c).

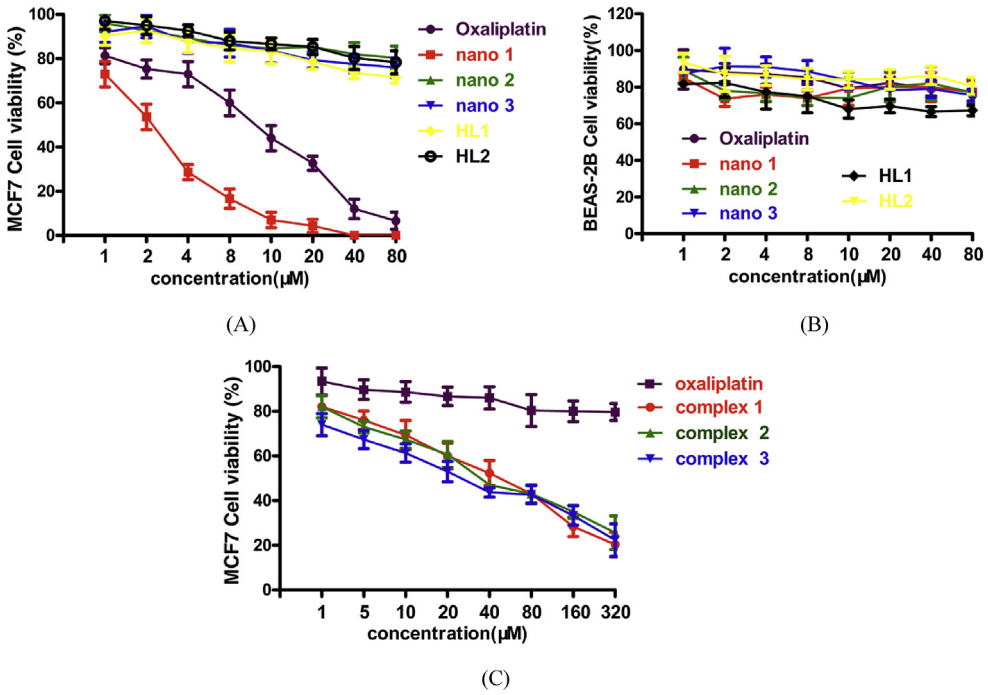

Fig. 6. Nanoparticle **1** restrains the proliferation and viability of MCF7 cells. (A) The survival curves of MCF7 cells treated with 1–3 nanoparticles and ligands (1,2,4,8,10,20,40,80,100 μM) for 24 h were plotted by CCK8 method.(B) normal lung cell line BEAS-2B were treated with the same consistence of ligands and nanoparticles **1**–**3**, CCK-8 method was used to measure cell viability. (C) The MCF7 cell viability curves after treated with complexes **1**–**3** determined by CCK-8. The data were expressed as three independent experiments mean ± SD.

molecule (calcd 9.87%). After 142 °C, 20% of the weight loss could be found to drop sharply owing to the decomposition of the discrete structure. Complex **2** TGA profile shows that a weight loss rate of 10.2% from room temperature to 167 °C, this is related to the escape of one lattice EtOH molecule. The framework could be stable up to the temperature of 170 °C. The thermogravimetric data plot of complex **3** shows a 10.8% weight loss started from the temperature of 25 °C till the temperature of 195 °C, it could be considered that

Table 2
IC_{50} value of nanoparticles **1**–**3,** complexes **1**–**3** and ligands (μM).

Cell/drug	Oxaliplatin	Nanoparticle 1	Nanoparticles 2	Nanoparticles 3	Complex 1	Complex 2	Complex 3	HL1	HL2
MCF7	9.11 ± 0.21	2.02 ± 0.08	>70	>70	43.63 ± 2.01	39.53 ± 1.64	22.21 ± 1.31	>70	>70
BEAS-2B	>70	>70	>70	>70	–	–	–	>70	>70

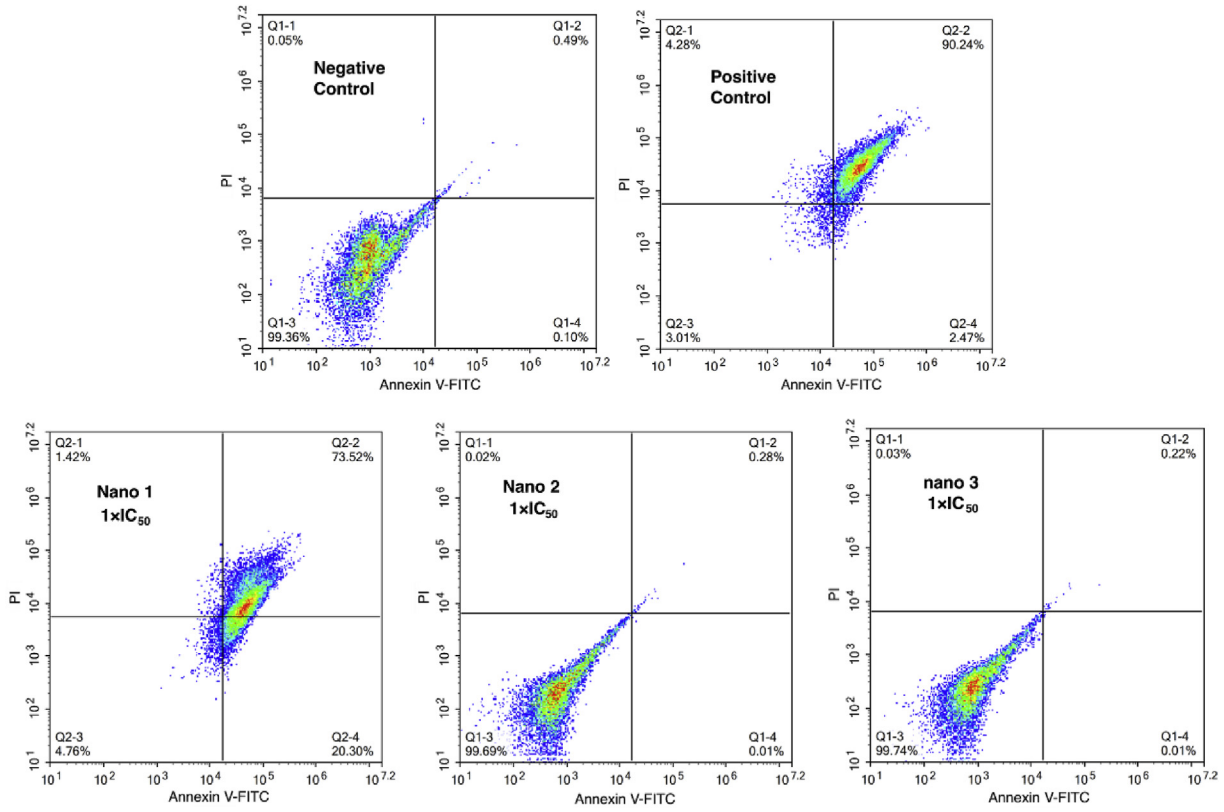

Fig. 7. Nano **1** promotes the MCF7 cell apoptosis and cell cycle arrest. Using **1**–**3** (1 × IC_{50}) nanoparticles specified doses to treat the MCF7 cancer cells for 24 h. (A) the cell apoptosis was detected by Annexin V-FITC apoptosis detection kit in flow cytometry. (B) Flow cytometry was used to quantitatively evaluate and analyze the distribution of cell cycle. Each group was repeated three times. The results were represented as three independent experiments means ± SD. Compared with the control group, $^{*}p < 0.05$ was obviously different.

this is due to the weightlessness of two lattice MeOH molecules. The extra part is due to the other parts of the molecule are disintegrated at such high temperatures. It need to be pointed out that the decomposition temperature of complex **3** is higher than that of complex **1**, which is due to the stronger chelating ability of tri-nucleating HL_2 ligand.

In light of the following bioactivity evaluation, it is necessary to make the above coordination complexes with micron dimension (Fig. S3) into nano-scale, which could promote drug release to the whole body and absorbed by specific tissues through intravenous

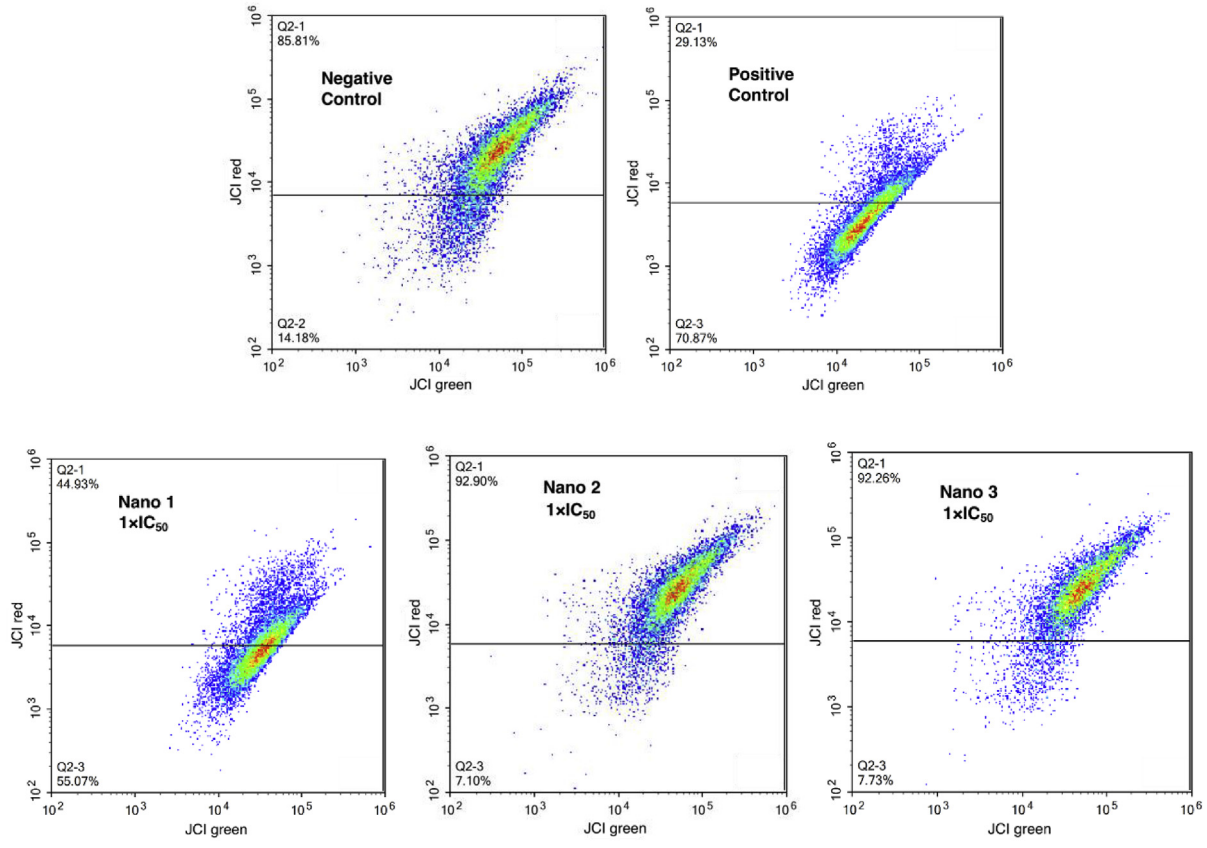

(A)

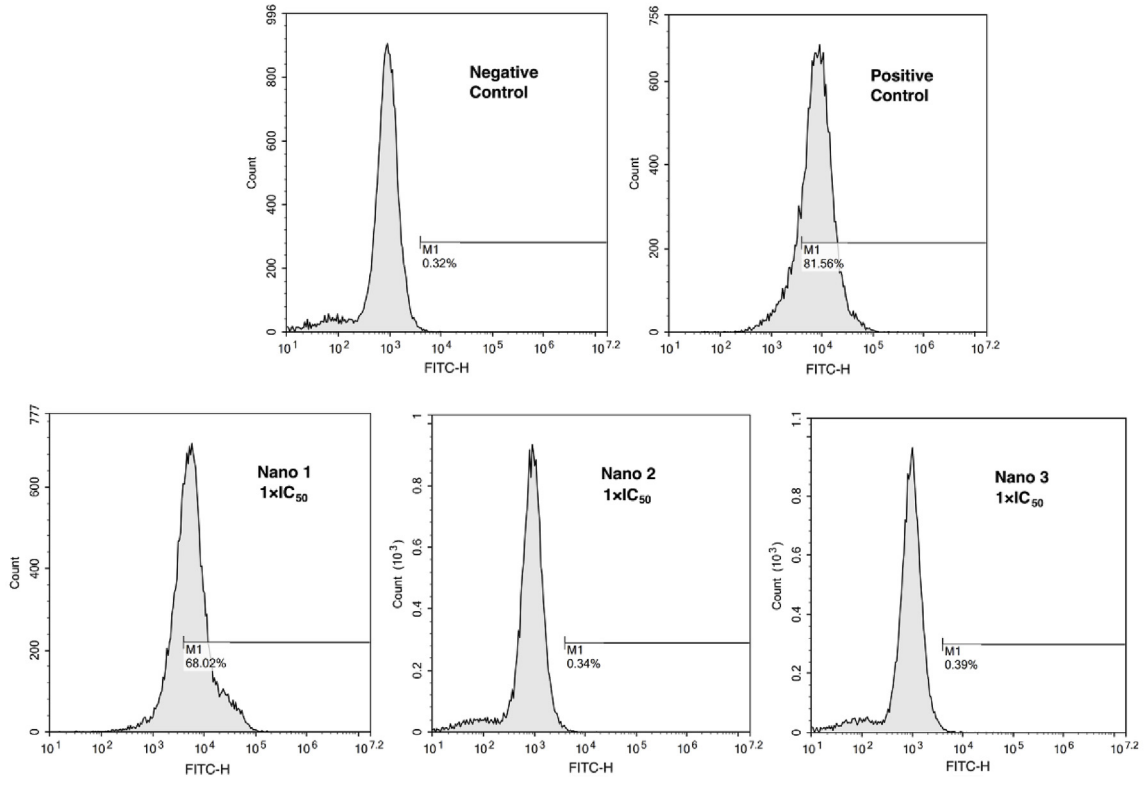

(B)

Fig. 8. Nano **1** triggers mitochondrial fragmentation and intracellular ROS accumulation. Using **1**–**3** ($1 \times IC_{50}$) nanoparticles to treat the MCF7 cancer cells with 70%–80% confluence for 24 h. (A) The ratio of JC-1 aggregates to JC-1 monomers in MCF7 cancer cells treated with different nanoparticles 1–3 was studied. (B) Using ROS detection kit to quantitatively analyzed ROS content in MCF7 cancer cells.

injection. Interestingly, for single crystals of complexes **1**–**3** when subjected to a mechanical grinding in a mortar and pestle for about 30 min, crystalline nanoscale complexes were obtained. Powder X-ray diffraction (PXRD) studies confirm the crystalline properties of nanomaterials. It is also observed that PXRD patterns of these nanocompounds completely match with bulk PXRD patterns and simulation of corresponding complexes. The production of the nanoparticles was further evidenced through SEM researches that are acquired via dropping nanoparticles in DMSO dispersion solution on glass surface. The morphology of particles for complexes is observed as spherical for nanoparticle **1**, sheet form for the nanoparticles **2**–**3**. The average size for the nanoparticle **1** is around 170 nm and the average thickness for the complexes **2** and 3 is 48 nm and 76 nm, respectively (Fig. 5).

3.3. Anti-viability activity of nano 1 in MCF7 cancer cells

In order to study the inhibition of nanoparticles **1**–**3** on the activity and proliferation in MCF7 cancer cells, the CCK-8 cell proliferation test was carried out. As results shown in Fig. 6A, the compound reduced the proportion of viable MCF7 cells with a dose-dependent method, Unexpectedly, nanoparticles **2**–**3** showed no inhibitory effect on MCF7 cancer cells growth. All the three nanos have no cytotoxicity on normal lung cell line BEAS-2B cells (Fig. 6B). To exclude the influence of HL1 and HL2 ligand on the inhibitory effect of nanoparticles **1**–**3** against cancer cells viability, the cytotoxicity of HL1 and HL2 was also measured by CCK-8 assay, as results showed in Fig. 6A and B, HL1 and HL2 have no effect on cell growth. The anticancer activity of complexes **1**–**3** was measured and showed in Fig. 6C, which reflected that the complexes **1**–**3** also showed anticancer activity but they are obvious lower than those of the nanoparticles **1**–**3**, highlighting the advantages of the formation of the nanoparticles.

The IC_{50} values of nanos, complexes and ligands were computed by SPSS 22.0, the results were showed in Table 2. The IC_{50} value of nanoparticle **1** is $2.02 \pm 0.08\ \mu M$, which has remarkable antiproliferative activity for human breast cancer. The dose of $1 \times IC_{50}$ was chosen for the subsequent experiments.

3.4. Nano 1 induces MCF7 cell death and cell cycle arrest

Most anticancer drugs play an anticancer role by causing apoptosis. To investigate whether nano **1** induce the MCF7 cancer cell death via the apoptotic manner, the Annexin V-FITC/PI double staining assay was conducted. The MCF7 cancer cells was detected by **1**–**3** nanoparticles at indicated concentrations 24 h for apoptosis detection. The Annexin V/PI staining results showed that, after incubated with nanoparticle **1**, the apoptosis rate in nano **1** treatment group was significantly higher than other treatment groups and the control group (Fig. 7A), indicating that nano **1** activated the process of MCF7 cancer cell apoptosis.

3.5. Nano 1 causes ROS accumulation by triggering mitochondrial fragmentation

$\Delta\psi m$ is known as the indicator of cell damage, it would decrease combined with the damage of mitochondrial membrane. In order to detect the changes of MMP, a marker of apoptosis, MCF7 cancer cells were dyed with JC-1 fluorescent dye and analyzed by flow cytometry [17]. After treated with indicated concentrations of nanoparticle **1**, increased percentage of JC-1 stained green and existed in monomeric form, which indicated MMP decreased under nanoparticle **1** treatment (Fig. 8A).

The damage of mitochondrial membrane causes accumulating of ROS in cells, which has the important function in apoptosis [18]. We speculated the nano **1** might increase the level of ROS and ultimately induce apoptosis of MCF7 cells. According to the result shown in Fig. 8B, the nano **1** significantly increased intracellular ROS accumulation, and the ROS level was not changed in the nanoparticles **2**–**3** treatment group. These results suggest that only nanoparticle **1** can induce the death of MCF7 cells, combined with ROS accumulation and mitochondrial death in human breast cancer cells.

4. Conclusion

In summary, we have successfully prepared two Schiff base ligands 2-((ethylamino)methyl)-6-methoxyphenol (HL_1) and (E)-2-(((2-(dimethylamino)ethyl)imino)methyl)-6-methoxyphenol (HL_2) with different amount of chelating donors, which are further used in the synthesis of three novel Ni(II)-based and Cu(II) coordination complexes with various coordination surroundings for the center metal ions. In addition, the green manual grinding technology has been used to decrease the particle diameter of complexes **1**–**3**, thus forming nano-complexes. Besides, we also found that nanoparticles **1** had anticancer activity against human breast cancer cells using CCK-8 detection kit with the IC_{50} value in the range of micromolar. This study offers the evidence of nanoparticle **1** appear causes obvious mitochondrial fragmentation in MCF7 cancer cells, which then initiated the intracellular ROS accumulation and finally caused the cancer cell apoptosis. In conclusion, nanoparticle **1** is likely to be an anticancer agent for human breast cancer treatment.

Appendix A. Supplementary data

Supplementary data to this article can be found online at https://doi.org/10.1016/j.molstruc.2019.126938.

References

[1] L. Kang, L. Zhao, S. Yao, C. Duan, Ceram. Int. 45 (2019) 16717.
[2] X. Feng, Y.Q. Feng, J.L. Chen, L.Y. Wang, Dalton Trans. 44 (2015) 804.
[3] C. Duan, F. Li, M. Yang, H. Zhang, Y. Wu, H. Xi, Ind. Eng. Chem. Res. 57 (2018) 15385.
[4] X. Feng, L.F. Ma, L. Liu, S.Y. Xie, L.Y. Wang, Cryst. Growth Des. 13 (2013) 4469.
[5] Y.Y. Yang, L. Kang, H. Li, Ceram. Int. 45 (2019) 8017.
[6] X. Feng, L.Y. Wang, J.-S. Zhao, J.G. Wang, S.W. Ng, B. Liu, X.G. Shi, CrystEngComm 12 (2010) 774.
[7] R.M. McQuade, V. Stojanovska, J.C. Bornstein, K. Nurgali, Curr. Med. Chem. 24 (2017) 1537.
[8] M. Zhang, C. Saint-Germain, G. He, R.W.Y. Sun, Curr. Med. Chem. 25 (2018) 493.
[9] W.F. De Azevedo Jnr, Y.P. Mascarenhas, G.F. De Sousa, C.A.L. Filgueiras, Acta Crystallogr. Sect. C Cryst. Struct. Commun. 51 (1995) 619.
[10] A.M. Florea, D. Büsselberg, Cancers 3 (2011) 1351.
[11] P.C. Bruijnincx, P.J. Sadler, Curr. Opin. Chem. Biol. 12 (2008) 197.
[12] I. Bernadette Amali, M.P. Kesavan, V. Vijayakumar, N. Indra Gandhi, J. Rajesh, G. Rajagopal, J. Mol. Struct. 1183 (2019) 342.
[13] C. Kachi-Terajima, T. Shimoyama, T. Ishigami, M. Ikeda, Y. Habata, Dalton Trans. 47 (2018) 2638.
[14] J. Zhang, L. Xu, W.Y. Wong, Coord. Chem. Rev. 355 (2018) 180.
[15] P. Ghorai, R. Saha, S. Bhuiya, S. Das, P. Brandão, D. Ghosh, T. Bhaumik, P. Bandyopadhyay, D. Chattopadhyay, A. Saha, Polyhedron 141 (2018) 153.
[16] V. Torabi, H. Kargar, A. Akbari, R. Behjatmanesh-Ardakani, H. Amiri Rudbari, M. Nawaz Tahir, J. Coord. Chem. 71 (2018) 3748.
[17] V.R. Chandrasekhar, K. Mookkandi Palsamy, R. Lokesh, D.T.T., I.G.N., R. Jegathalaprathaban, R. Gurusamy, Appl. Organomet. Chem. 71 (2018), e4753.
[18] W.Y. Lu, H.W. Ou, C.N. Lee, J.K. Vandavasi, H.Y. Chen, C.C. Lin, Polymer 139 (2018) 1.
[19] L.H. Abdel-Rahman, A.M. Abu-Dief, R.M. El-Khatib, S.M. Abdel-Fatah, J. Photochem. Photobiol. B Biol. 162 (2016) 298.
[20] F. Zhao, W. Wang, W. Lu, L. Xu, S. Yang, X.M. Cai, M. Zhou, M. Lei, M. Ma, H.J. Xu, F. Cao, Eur. J. Med. Chem. 146 (2018) 451.
[21] I. Ali, W.A. Wani, K. Saleem, M.F. Hseih, Polyhedron 56 (2013) 134.
[22] P. Tyagi, S. Chandra, B.S. Saraswat, Spectrochim. Acta Part A Mol. Biomol. Spectrosc. 134 (2015) 200.
[23] M.K. Rauf, S. Yaseen, A. Badshah, S. Zaib, R. Arshad, Imtiaz-ud-Din, M.N. Tahir, J. Iqbal, JBIC J. Biol. Inorg. Chem. 20 (2015) 541.

[24] J. Du Bois, C.S. Tomooka, J. Hong, E.M. Carreira, M.W. Day, Angew Chem. Int. Ed. Engl. 36 (1997) 1645.
[25] G.M. Sheldrick, Acta Crystallogr. Sect. C Struct. Chem. 71 (2015) 3.
[26] A.L. Spek, Acta Crystallogr. Sect. C Struct. Chem. 71 (2015) 9.
[27] T.K. Prasad, M.V. Rajasekharan, Cryst. Growth Des. 8 (2008) 1346.
[28] B. Ge, H. Liu, Q. Liang, L. Shang, T. Wang, S. Ge, Arch. Oral Biol. 99 (2019) 126.
[29] A. Kawiak, E. Lojkowska, PLoS One 11 (2016), e0147718.
[30] B. Yu, X. Ye, Q. Du, B. Zhu, Q. Zhai, X.X. Li, Cell. Physiol. Biochem. 41 (2017) 2489.
[31] A. Ray, S. Jena, B. Dash, A. Sahoo, B. Kar, J. Patnaik, P.C. Panda, S. Nayak, N. Mahapatra, Cancer Manag. Res. 11 (2019) 483.
[32] W. Liu, H.H. Thorp, Inorg. Chem. 32 (1993) 4102.
[33] L.S. Kau, D.J. Spira-Solomon, J.E. Penner-Hahn, K.O. Hodgson, E.I. Solomon, J. Am. Chem. Soc. 109 (1987) 6433.
[34] L. Yang, D.R. Powell, R.P. Houser, Dalton Trans. 109 (2007) 955.
[35] J. Gaazo, Coord. Chem. Rev. 19 (1976) 253.